The Astronomical Journal, 129:2203–2216, 2005 May

THE COMPLEX STAR FORMATION HISTORY OF NGC 1569[1]

L. Angeretti
Dipartimento di Astronomia, Università di Bologna, via Ranzani 1, I-40127 Bologna, Italy; luca.angeretti@bo.astro.it

M. Tosi
INAF–Osservatorio Astronomico di Bologna, via Ranzani 1, I-40127 Bologna, Italy; monica.tosi@bo.astro.it

L. Greggio
INAF–Osservatorio Astronomico di Padova, vicolo dell'Osservatorio 5, I-35122 Padua, Italy; greggio@pd.astro.it

E. Sabbi
Dipartimento di Astronomia, Università di Bologna, via Ranzani 1, I-40127 Bologna, Italy; elena.sabbi@bo.astro.it

and

A. Aloisi[2] and Claus Leitherer
Space Telescope Science Institute, 3700 San Martin Drive, Baltimore, MD 21218; aloisi@stsci.edu, leitherer@stsci.edu
Received 2004 August 10; accepted 2005 February 13

ABSTRACT

We present new results on the star formation history of the dwarf irregular galaxy NGC 1569. The data were obtained with the *Hubble Space Telescope* NICMOS/NIC2 in the F110W (J) and F160W (H) near-infrared (NIR) filters and interpreted with the synthetic color-magnitude diagram method. The galaxy has experienced complex star formation (SF) activity. The best fit to the data is found by assuming three episodes of activity in the last 1–2 Gyr. The most recent and strong episode constrained by these NIR data started $\sim 3.7 \times 10^7$ yr ago and ended $\sim 1.3 \times 10^7$ yr ago, although we cannot exclude the possibility that up to three SF episodes occurred in this time interval. The average star formation rate (SFR) of the episode is $\sim 3.2\ M_\odot\ \mathrm{yr}^{-1}\ \mathrm{kpc}^{-2}$, in agreement with literature data. A previous episode produced stars between $\sim 1.5 \times 10^8$ and $\sim 4 \times 10^7$ yr ago, with a mean SFR about two-thirds lower than the mean SFR of the youngest episode. An older SF episode occurred about 1×10^9 yr ago. All these SFRs are 2–3 orders of magnitude higher than those derived for late-type dwarfs of the Local Group. In all cases an initial mass function similar to Salpeter's allows for a good reproduction of the data, but we cannot exclude flatter mass functions. These results have been obtained adopting a distance of 2.2 Mpc and a reddening $E(B - V) = 0.56$. A larger distance would require younger episodes and higher SFRs. We have explored some possible scenarios using the astrated mass in the best-fit model, in order to constrain the past star formation history. We cannot rule out a low past SFR, but we can safely conclude that the last 1–2 Gyr have been peculiar.

Key words: galaxies: dwarf — galaxies: evolution — galaxies: individual (NGC 1569) — galaxies: irregular — galaxies: starburst — galaxies: stellar content

Online material: color figures

1. INTRODUCTION

In the last decade the field of galaxy evolution has gained substantial momentum, owing to the wealth of high-quality multiwavelength surveys from the main ground- and space-based telescopes and sophisticated theoretical models. Nonetheless, the current knowledge of the major physical mechanisms for galaxy formation and evolution is still affected by serious uncertainties. Traditionally, star formation (SF) in cosmology and galaxy formation studies is naively described by simple universal laws, and the stellar initial mass function (IMF) is assumed to be constant in time and space. The only way to obtain detailed information on these crucial evolution parameters is to study the stellar populations of nearby galaxies and derive the SF history (SFH) over cosmological timescales. One of the fundamental tools is the color-magnitude diagram (CMD) of the galaxies resolved into single stars. Since all the CMD features are related to the evolutionary state of the stellar populations, we can understand the SFH of a certain region within a galaxy by interpreting its CMD in terms of stellar evolution theory with the method of synthetic CMDs. In theory, from the CMD we can infer how many bursts have occurred, their duration and star formation rate (SFR), and the initial mass function (Tosi et al. 1991; Greggio et al. 1998) for any star formation law and metallicity. In practice, observational errors and theoretical uncertainties impose severe restrictions. The requirement of resolving a galaxy into stars limits the exploration of the SFH to nearby galaxies. At present, even the largest telescopes only permit such studies for galaxies with distances <15–20 Mpc, i.e., in the local universe. In this limited space volume we find many spirals and a plethora of both late and early dwarf galaxies.

Dwarf irregular galaxies (dIrrs) and blue compact galaxies (BCDs) play a major role in the field of galaxy evolution (Grebel 1997; Mateo 1998). With their high gas content and low metallicity, they could be similar to primeval galaxies (Izotov et al. 1997) and the best possible sites for determining the primordial ^{4}He abundance (Izotov & Thuan 2004; Olive & Skillman 2004). It has been suggested that the excess of number counts of faint blue galaxies at redshift $z \sim 1$ may be ascribed to dwarf galaxies

[1] Based on observations with the NASA/ESA *Hubble Space Telescope*, obtained at the Space Telescope Science Institute, which is operated by Association of Universities for Research in Astronomy, Inc., for NASA under contract NAS5-26555.

[2] On assignment from the Space Telescope Division of the European Space Agency.

undergoing their first burst of SF (Ellis 1997). Dwarf galaxies are important in galaxy formation models, since in hierarchical models they are assumed to be the building blocks from which other types of galaxies form through merging.

Key questions on the evolution of late-type dwarfs are: did all the dIrrs and BCDs experience SF in the past? If so, what are the properties of the SF episodes? Several stellar population studies have suggested that dIrrs are characterized by a gasping (episodes of moderate activity separated by short quiescent phases) SF with no evidence of extended gaps (Tosi et al. 1991; Schulte-Ladbeck et al. 2001; Dolphin et al. 2003; Skillman et al. 2003). Their SFR is not strong enough to explain the faint galaxy counts excess.

NGC 1569 is a dIrr near the Local Group. Its intrinsic distance modulus (DM) has been estimated to be 26.71 ± 0.60 (Arp & Sandage 1985; Israel 1988; Waller 1991), corresponding to a distance of 2.2 ± 0.6 Mpc. O'Connell et al. (1994) obtained a distance modulus of 27.0 ± 0.5, corresponding to 2.5 ± 0.5 Mpc, while Karachentsev et al. (1994) and Richer & McCall (1995) found 1.8 ± 0.4 and $\sim$1.7 Mpc, respectively. Recently, Makarova & Karachentsev (2003) derived a new distance to NGC 1569 based on the I magnitude of the tip of the red giant branch (RGB). Their data are consistent with two possible distances: 1.95 ± 0.2 or 2.8 ± 0.2 Mpc. Hereafter, we adopt a distance of 2.2 ± 0.6 Mpc (Israel 1988), which encompasses the wide range of distances proposed in the literature.

The low Galactic latitude ($b = 11\overset{\circ}{.}2$) of NGC 1569 implies significant Galactic reddening. Burstein & Heiles (1984) estimated a value of $E(B-V) = 0.51$ for the foreground extinction using the H I column density. Israel (1988) found a total extinction of $E(B-V) = 0.56 \pm 0.10$ from the UV color-color diagram. Furthermore, many authors have suggested the existence of a strong, differential, internal reddening. Gonzalez-Delgado et al. (1997) found a total reddening of $E(B-V) = 0.67 \pm 0.02$ in the direction of the super star clusters (SSCs), where the component of the intrinsic reddening is $E(B-V) = 0.11$. Devost et al. (1997) estimated the Galactic extinction to be $E(B-V) = 0.50$ and the intrinsic mean extinction $E(B-V) = 0.20$, using optical emission spectra of the ionized gas in NGC 1569. Kobulnicky & Skillman (1997) found a variation of the total reddening in the galaxy from $E(B-V) \simeq 0.51$ to $\simeq$0.77 with an average value $E(B-V) \simeq 0.63$ (with $R = 3.1$). They found it reasonable to assume a Galactic foreground of $E(B-V) = 0.51$ and ascribe the difference to the internal reddening. In Kobulnicky & Skillman (1997), the extinction for the area discussed in the present paper is $E(B-V) \sim 0.58$, except for the SSCs and H II regions. Origlia et al. (2001) derived a foreground extinction of $E(B-V) = 0.55 \pm 0.05$ and an intrinsic reddening of $E(B-V) = 0.15 \pm 0.05$ from UV spectra. The simulations presented in this paper assume $E(B-V) = 0.56 \pm 0.10$ (Israel 1988).

The mean oxygen abundance of NGC 1569 found in the literature is $12 + \log(\mathrm{O/H}) \simeq 8.2 \pm 0.2$ dex. With an assumed $[\mathrm{O/Fe}] = 0.0$, the average metallicity is then $0.25\ Z_\odot$, corresponding to $Z \sim 0.004$ (see Greggio et al. 1998 and references therein) if $Z_\odot = 0.02$.[3]

This rather exceptional dwarf galaxy is known to contain two SSCs, SSC-A and SSC-B, with SSC-A having two components, A1 and A2 (De Marchi et al. 1997; Origlia et al. 2001). Many H II regions are observed in those zones where SF is currently active (Waller 1991). Nevertheless, NGC 1569 is considered a "post" star-forming galaxy with a total dynamical mass of $M_{\rm dyn} \sim 3.3 \times 10^8\ M_\odot$ (Israel 1988), one-third of which is neutral hydrogen gas ($M_{\rm H\,I} \sim 1.3 \times 10^8\ M_\odot$; Stil & Israel 2002). This galaxy is a gas-rich system in a relatively early stage of chemical evolution. Many filaments are found at different wavelengths, and there is a strong spatial correlation between the extended X-ray emission and the H α filaments (Martin et al. 2002). The H I emission of NGC 1569 shows a dense, clumpy ridge distribution surrounded by a more extended diffuse neutral hydrogen. There are discrete features such as arms and bridges (Stil & Israel 2002). In the IR, Lisenfeld et al. (2002) found both large and very small grains exposed to a strong radiation field. Galliano et al. (2003) found different dust properties in NGC 1569 (most of the grains are small) compared to other more metal-rich galaxies. These results are consistent with the presence of shocks having dramatic effects on the dust. In the optical, deep Hα images show filaments and arcs of warm ionized gas. These filaments have a length of several kiloparsecs with typical velocities around 50–100 km s^{-1}. The highest velocities, up to 200 km s^{-1}, have been attributed to expanding superbubbles with dynamical ages of 10 Myr (Waller 1991) generated by a strong SF episode. At high energy, X-ray observations reveal that $\sim$60% of the soft X-ray emission in NGC 1569 is centered between the two SSCs. Its origin is attributed to thermal emission from the hot gas of a galactic superwind emanating from the disk (Heckman et al. 1995). *Chandra* observations find many high-mass X-ray binary systems and large inhomogeneities in the metal abundances of the interstellar medium (ISM) with ranges from 0.1 to 1 $Z_\odot$ (Martin et al. 2002). This is evidence that the ISM has been affected by numerous supernova explosions from a recent SF episode (Martin et al. 2002). Hydrodynamic simulations of D'Ercole & Brighenti (1999) demonstrated that a galactic wind triggered only by Type II supernova explosions (i.e., without stripping or other environmental effects) would not be very effective in removing the ISM in NGC 1569. In fact, even if most of the metal-rich stellar ejecta can be efficiently expelled from the galaxy and dispersed in the intergalactic medium, cold and dense gas replenishes the central region of the galaxy a few hundred million years after the starburst.

The SFH of NGC 1569 has most recently been studied by two groups with *Hubble Space Telescope* (*HST*) data. In optical bands (V and I), Vallenari & Bomans (1996) found a global SF episode from 100 to 4 Myr ago and hints of an older episode of SF from 1.5 Gyr ago to 150 Myr ago. They ruled out the existence of long quiescent phases in the last 1.5 Gyr. Based on B and V data, Greggio et al. (1998, hereafter G98) found a global SF episode of $\gtrsim$0.1 Gyr duration, ending $\sim$5–10 Myr ago. During the burst, the SFR was approximately constant, and if quiescent periods occurred, they lasted less than $\sim$10 Myr. The derived SFR is very high and equal to 3, 1, or 0.5 $M_\odot$ yr^{-1} for a single-slope initial mass function[4] with an exponent $\alpha = 3$, 2.6, or 2.35, respectively, and a mass range from 0.1 to 120 $M_\odot$. From *HST* NICMOS images, Aloisi et al. (2001, hereafter AL01) found that young stars ($M > 8\ M_\odot$, age < 50 Myr) are more clustered around the two SSCs, while the intermediate-age objects ($1.9\ M_\odot < M < 8\ M_\odot$, 50 Myr $<$ age $<$ 1 Gyr) have an almost uniform distribution, and the old stars ($M < 1.9\ M_\odot$, age $>$ 1 Gyr) are located at the outskirts of the starbursting region.

All these studies show that NGC 1569 experienced a strong SFR in recent epochs. With a total mass of $\sim 3.3 \times 10^8\ M_\odot$, the system cannot have sustained such a strong activity over a Hubble time, since it would have consumed all the gas in less than 1 Gyr (G98). The question then is whether the SF in NGC 1569 has

[3] In recent years, the solar abundances have undergone major revisions (Asplund et al. 2004). The current estimate of the solar metallicity is $Z_{\odot,\rm new} = 0.013$.

[4] Throughout this paper we parameterize the IMF as $\varphi(m) \propto m^{-\alpha}$. In this notation, Salpeter's slope is $\alpha = 2.35$.

started only in relatively recent epochs or has lasted for several gigayears but at much lower rates. Our goal is to obtain a better understanding of the past history of this galaxy. The best way to study old stellar populations, at least in principle, is to observe in the IR bands where the RGB phase is more evident and where reddening effects are not as severe as in optical bands.

In this work, we derive the SFH with the synthetic CMD method (Tosi et al. 1991; G98) using the data of AL01 in the NIR filters. In § 2 we summarize the data and the observed CMD. In § 3 we briefly describe the CMD method and the artificial star experiment in order to derive completeness and photometric errors. The results are presented in § 4. They are discussed and compared with the literature in § 5.

2. FROM THE OBSERVATIONS TO THE CMD

We briefly summarize the main characteristics of the observations and photometric reductions; for further details, see AL01. The observations of NGC 1569 were performed in 1998 with the NICMOS/NIC2 camera on board *HST* in the F110W and F160W filters. The images cover the crowded central region of the galaxy, where SSC-A, SSC-B, cluster 30, and part of an extended H II region complex are present. The NIC2 camera has a field of view of $19\farcs2 \times 19\farcs2$, corresponding to 205 pc $\times$ 205 pc at a distance of 2.2 Mpc. The observations were taken with dithering. The resulting "drizzled" images have a point-spread function (PSF) FWHM of 3.0 and 3.9 pixels in F110W and F160W, respectively, and a pixel size of $0\farcs0375$, which corresponds to $\sim$0.4 pc.

The photometric reduction has been performed by AL01 using DAOPHOT via PSF fitting. PSF-fitting photometry is not the ideal procedure for drizzled images, because drizzle creates a position-dependent PSF smearing and produces correlated noise between adjacent pixels (Fruchter & Hook 2002). However, PSF-fitting is the only viable technique in a crowded field like the central region of NGC 1569. AL01 used the deepest image (F110W) to locate the stars and used their coordinates to force photometry in the F160W image. This implies that all of the objects detected in the F160W image are also present in F110W, but the opposite is not necessarily true. Then, they selected the objects by adopting the DAOPHOT parameters $\chi^2 < 1.5$ and sharpness <0.4 and obtained the final catalog of 3177 stars. The objects rejected by the selection criteria described above are typically the brightest objects in the SSCs, smaller star clusters, extended objects, and blends. The star magnitudes were calibrated in the *HST* VEGAMAG system.

The CMD and luminosity function (LF) for NGC 1569 derived by AL01 are plotted in Figure 1. The limiting magnitude is $m_{\rm F110W} \simeq 24.5$, and the color range is $m_{\rm F110W} - m_{\rm F160W} = -0.8-3$. To easily identify the main evolutionary phases, we plotted the Padova tracks (Fagotto et al. 1994) for a metallicity of $Z = 0.004$ on the same scale (Fig. 1). The dominant feature is the "red plume" extending from $m_{\rm F110W} \sim 18$ to $\sim$20.5. It has a small spread in color (0.2 mag) and a long range in magnitude. The region corresponds to the He-burning phases of stars with masses approximately from 9 to 20 $M_\odot$. The more massive stars in our catalog have masses of 15–20 $M_\odot$, corresponding to ages of 10–15 Myr. A second feature is defined by the bulk of objects with $m_{\rm F110W} \sim 21-24$ and $m_{\rm F110W} - m_{\rm F160W} > 0.9$, where the tip of the RGB could be located.

Unfortunately, the RGB feature is not recognizable in the observed CMD. The tip of the RGB should be located at $m_{\rm F110W} \simeq 22.4$ for an adopted DM = 26.71 and $E(B-V) = 0.56$. On the other hand, the DM uncertainty introduces an uncertainty of 0.6 mag in the location of the RGB tip (between 21.8 and 23.0 in $m_{\rm F110W}$). In addition, the RGB tip feature on the LF could be blurred in the CMD because the strong SF occurred at intermediate ages, as found by Vallenari & Bomans (1996) and this paper (see below).

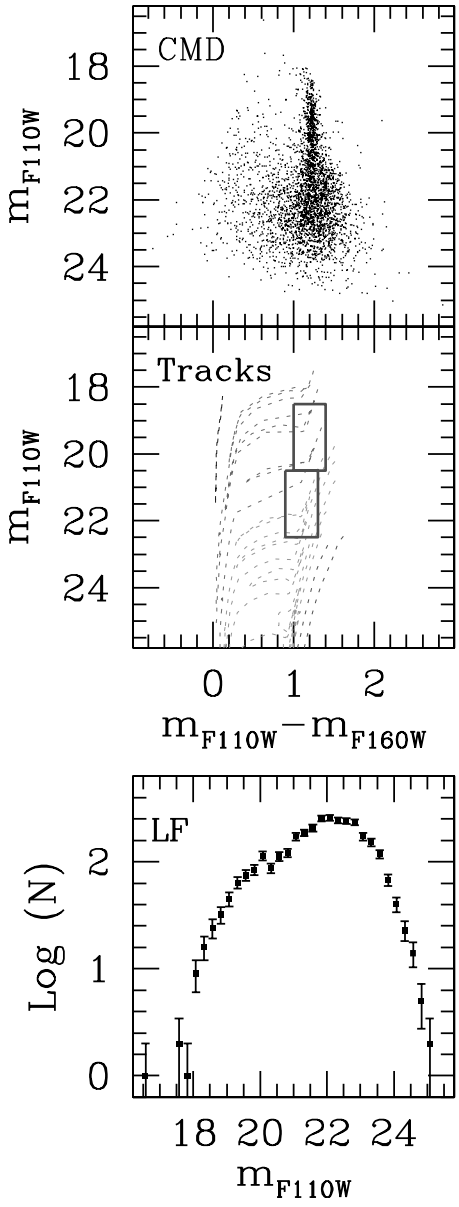

FIG. 1.—*Top*: Observed $m_{\rm F110W}$ vs. $m_{\rm F110W} - m_{\rm F160W}$ color-magnitude diagram. *Middle*: Padova tracks of metallicity $Z = 0.004$ for 1, 1.5, 1.7, 2, 2.5, 3, 4, 5, 6, 9, 15, 20, and 30 $M_\odot$ shown as dashed lines. The boxes described in the text are plotted with solid lines: BOX1 (18.5–20.5 and 1.0–1.4) and BOX2 (20.5–22.5 and 0.9–1.3). *Bottom*: Luminosity function with a step of 0.25 mag. [*See the electronic edition of the Journal for a color version of this figure.*]

3. FROM THE EMPIRICAL TO THE SYNTHETIC CMDS

The derivation of the SFH from the CMD is critically dependent on the completeness and analysis of the photometric errors. This is particularly true for the oldest populations in a crowded field such as the central region of NGC 1569, where blending of unresolved stars may severely affect our data and create spurious features in the derived CMD. It is therefore crucial to quantify these effects as well as possible by following the recipes of the data reduction and include them in the construction of the synthetic CMDs.

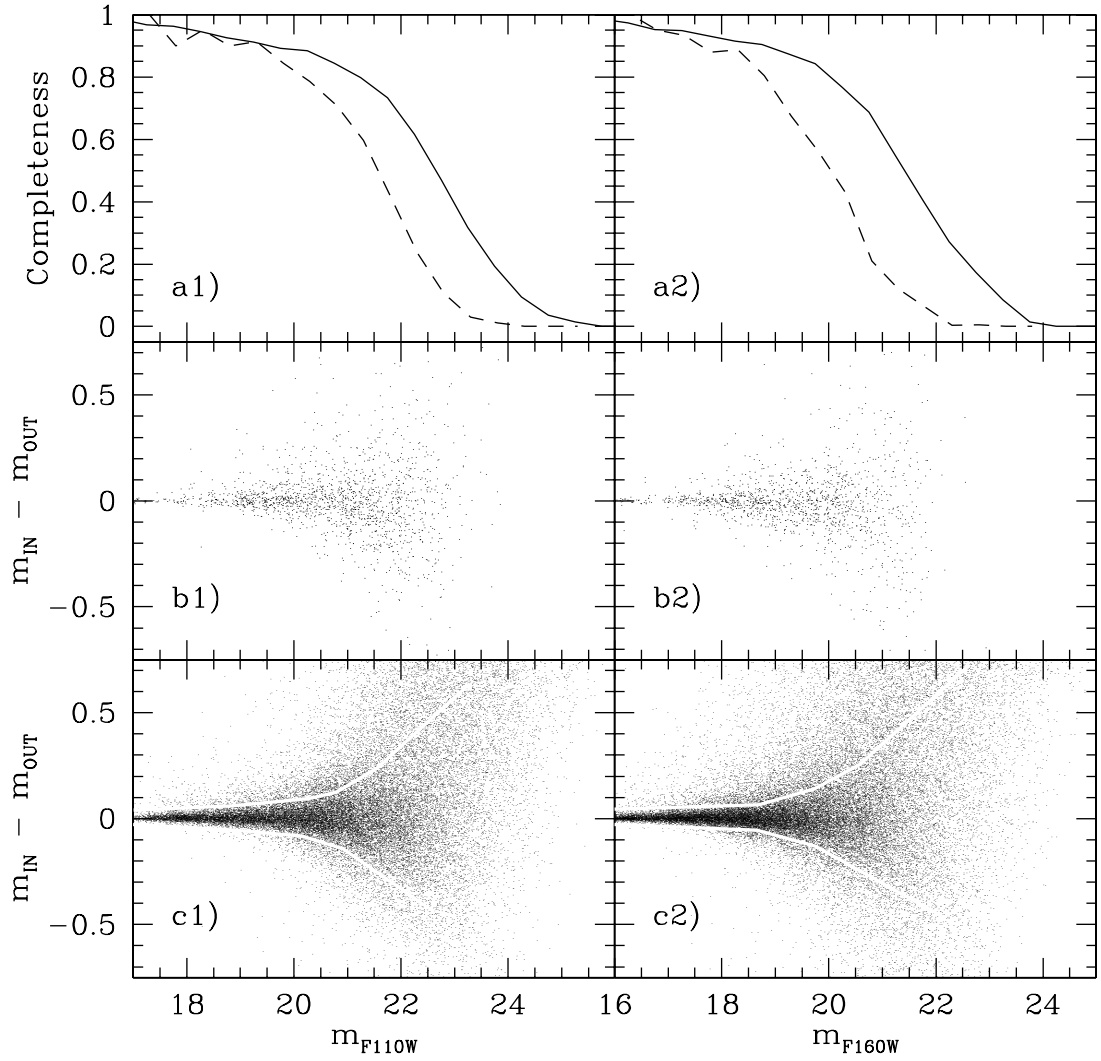

FIG. 2.—Results of the ASEs for the F110W (*left panels*) and F160W filters (*right panels*). The completeness functions are in the top panels. The solid lines refer to the completeness obtained in our study with Montegriffo's method described in Tosi et al. (2001), and the dashed lines are from AL01. In the middle panels we show the photometric error distributions derived by AL01, while the distributions obtained with Montegriffo's method are shown in the bottom panels. We indicate as thick lines the cuts in the error distributions adopted to perform the simulations presented in this paper.

3.1. *Artificial Star Experiments*

We accounted only for the completeness of the F160W frame in our simulations because, as mentioned above, all the stars detected in F160W were previously found in F110W. However, we have performed the artificial star experiment (ASE) in both images, since the photometric errors in both bands are required.

We initially adopted the ASE performed by AL01. They performed tests in which the fake stars have a PSF equal to that adopted in the data reduction. Then a fraction ($\sim$10%) of the number of detected stars was added at random positions on the image in each run and about 10 runs were performed. The total number of artificial stars was then similar to that of the detected objects. They derived an effective limiting magnitude of the data of $m_{\rm F160W} \simeq 23$ and a 50% completeness level at $m_{\rm F160W} \simeq 20$. In the top panels of Figure 2 we plot their completeness and photometric error distributions. The results obtained for $m_{\rm F160W}$ and $m_{\rm F110W}$ are shown in the right and left panels, respectively. In the top panels we plot the completeness factors from AL01 as dashed lines, while in the middle panels we draw their estimated photometric error distributions.

When we applied the ASE results from AL01 to the simulations, we found that they do not allow us to reproduce the faintest part of the CMD. For instance, if we simulate an old SF episode (starting 5×10^9 yr ago and still active) with the same number of stars of the observed CMD, we obtain a synthetic diagram that underproduces the faint ($m_{\rm F110W} \gtrsim 23.5$) tail of the LF by 50%. We interpret this result as being due to an underestimate of the true completeness in the AL01 ASE, and we therefore performed new ASE computations. We believe that this is because AL01's approach does not add a sufficient number of artificial stars at faint magnitudes, where crowding, blending, and incompleteness are very severe. We therefore adopted a procedure developed by P. Montegriffo at the Bologna Observatory (Tosi et al. 2001), which uses $\sim 10^5$ artificial stars per band. We have put fake stars in the images according to a LF similar to the observed one. At brighter magnitudes this LF follows the observed one, but at low luminosities a higher number of stars is required because of the high probability of losing objects because of crowding. All the fake stars have a PSF equal to that adopted in the actual data reduction. To avoid artificial crowding, we divided the frames in grids of cells of known width, and we randomly positioned only one fake star per cell at each run. We forced each star to have a distance from the cell edges large enough to guarantee that all its flux and background measuring regions fell within the cell. In

this way, we could control the minimum distance between adjacent stars. At each run, the position of the grid is randomly changed, and the artificial stars are then searched in the image by using the same procedure adopted for the real data and selected with the same criteria.

An artificial star was considered lost when the difference between the input and output magnitude was larger than 0.75. Such a difference implies that the artificial star overlaps with another star of the same luminosity or brighter. In the top panels of Figure 2, the completeness derived using Montegriffo's method is shown as a solid line. The photometric error distributions are plotted in the bottom panels as dots. The effective limiting magnitude of the data is $m_{\rm F160W} \simeq 24.5$, and the sample is 50% complete at $m_{\rm F160W} \simeq 21.5$. We found a posteriori that the completeness function obtained with Montegriffo's method allows us to reproduce the faint LF significantly better than with the previous ASE.

The input-output magnitude difference of the artificial stars provides an estimate of the photometric errors, which is safer than the error indicators of the reduction package ($\sigma_{\rm DAOPHOT}$ in our case). The outcomes are plotted in Figures 2*b* and 2*c* for the ASE approaches by AL01 and Montegriffo, respectively. The synthetic CMDs obtained by adopting the photometric errors from the artificial star tests usually reproduce the color and magnitude spread of the observational CMDs very well (see, e.g., Gallart et al. 2002; Smecker-Hane et al. 2002; Tosi et al. 2002; Annibali et al. 2003). In this case, however, by adopting the input-output magnitude difference of Figure 2*b* as photometric error, we obtain an excessively large color spread in the sequences of the synthetic CMD. This effect is clearly evident along the red plume, where the observed CMD is tight in color. We therefore used the synthetic CMDs to heuristically infer the appropriate error distribution in each filter. First, we cut the wings of the photometric error distributions at the 1 σ level in each magnitude bin and adopted these distributions to derive a test CMD. Since in this test CMD the 1 σ photometric error still has a color distribution larger than observed, we iterated the cutting procedure until we obtained photometric error distributions capable of reproducing the spread in the main features of the CMD. The cuts performed on the photometric error distributions eventually adopted are those shown within the solid lines in the bottom panels of Figure 2.

3.2. *Preliminary Tests*

We have also checked whether different portions of the image have different completeness and photometric errors. To this end, we have divided the NIC2 images into three regions: the central one covering the most crowded part of the image including the SSCs and the other two toward the edges in opposite directions. No relevant deviation has been found either in the completeness factors or in the input-output magnitude difference of the three regions.

Many authors have found evidence of spatially variable intrinsic extinction in NGC 1569; this extinction increases toward the central region of the galaxy, where SSCs and H II regions are located (Gonzalez-Delgado et al. 1997; Devost et al. 1997; Kobulnicky & Skillman 1997; Origlia et al. 2001). We have divided the image into subregions and compared the corresponding color functions in order to investigate whether strong differential reddening is present in our field. No significant differences in the color distributions have been detected from the image center to the edges. We are confident that differential reddening is not an issue in our 205 pc$\times$205 pc sized region.

Since the CMDs of all the subregions show similar photometric errors, completenesses, and color distributions, we have derived a global SFH over the whole 205 pc$\times$205 pc image.

3.3. *The Synthetic CMD Method*

The synthetic CMDs are constructed via Monte Carlo extractions of (mass, age) pairs, according to an assumed IMF, SF law, and initial and final epoch of the SF activity. Each synthetic star is placed in the theoretical $\log (L/L_{\odot})$, $\log T_{\rm eff}$ plane by suitable interpolations on the adopted evolutionary tracks (in this case, the Padova sets by Fagotto et al. 1994). Luminosity and effective temperature are transformed into the desired photometric system by interpolation within appropriate tables for photometric conversions (the transformations to the VEGAMAG system by Origlia & Leitherer 2000 in this case), and the resulting absolute magnitude is converted to a provisional apparent magnitude by applying reddening and distance modulus. An incompleteness test on the F160W magnitudes is then performed, based on the results from Montegriffo's ASE. A photometric error is assigned to all the retained stars by using the "modified distributions" discussed in § 3.1. The value of the SFR is obtained when the number of objects in the synthetic CMD (or in regions corresponding to specific evolutionary phases) is consistent with the observational data. When the examined CMD region contains only a few objects, we perform several simulations in order to avoid problems due to small number statistics. In these cases, we adopted the average value of the resulting SFRs.

4. SIMULATIONS

In order to derive the SFH of a galaxy, we explore a parameter space dependent on the distance modulus, reddening, IMF, SF law, metallicity, and age of the episodes. We obtain a solution when we have a combination of parameters that generate a synthetic CMD similar to the observed one. The exploration is also limited by the intrinsic uncertainties of the theoretical models, like those introduced by the stellar evolution tracks and the photometric conversions.

First, we attempt to reproduce the observed CMD with a single episode and metallicity model over the whole range of ages covered by the empirical CMD. If a single episode does not reproduce the observed CMD, we assume multiple SF events. If a single metallicity does not allow us to simulate an acceptable CMD, we try to change the metallicity for each episode. Then we perform other simulations in order to check the effect on the resulting SFH by assuming different IMFs, distance moduli, and reddenings.

This approach gives us an indication of the uncertainty on the results of our simulations. It allows us to identify the range of parameter values leading to a satisfactory agreement with the data and to reject those clearly inconsistent with the observational evidence. Following this line of thought, we show the simulated episodes that fit the observed data but also some of the bad episodes, because they provide hints for a better understanding of the SFH. We ran more than 1000 simulations to infer the SFH of the complicated case of NGC 1569.

We first present the results obtained by adopting DM = 26.71, $E(B-V) = 0.56$, $Z = 0.004$, and a Salpeter (1955) IMF ($\alpha = 2.35$) over the whole mass range from 0.1 to 120 $M_{\odot}$. In § 4.3 we discuss the effect of assuming different values for the IMF slope, distance, and reddening parameters. The models all assume a constant SFR within the specific age ranges; we always report the SFR of each episode both in $M_{\odot}$ yr^{-1} kpc^{-2} and in $M_{\odot}$ yr^{-1} (the latter in brackets).

4.1. *Single-Episode SF*

We have run several cases with a single episode of SF in NGC 1569, all constrained to reproduce the total number of

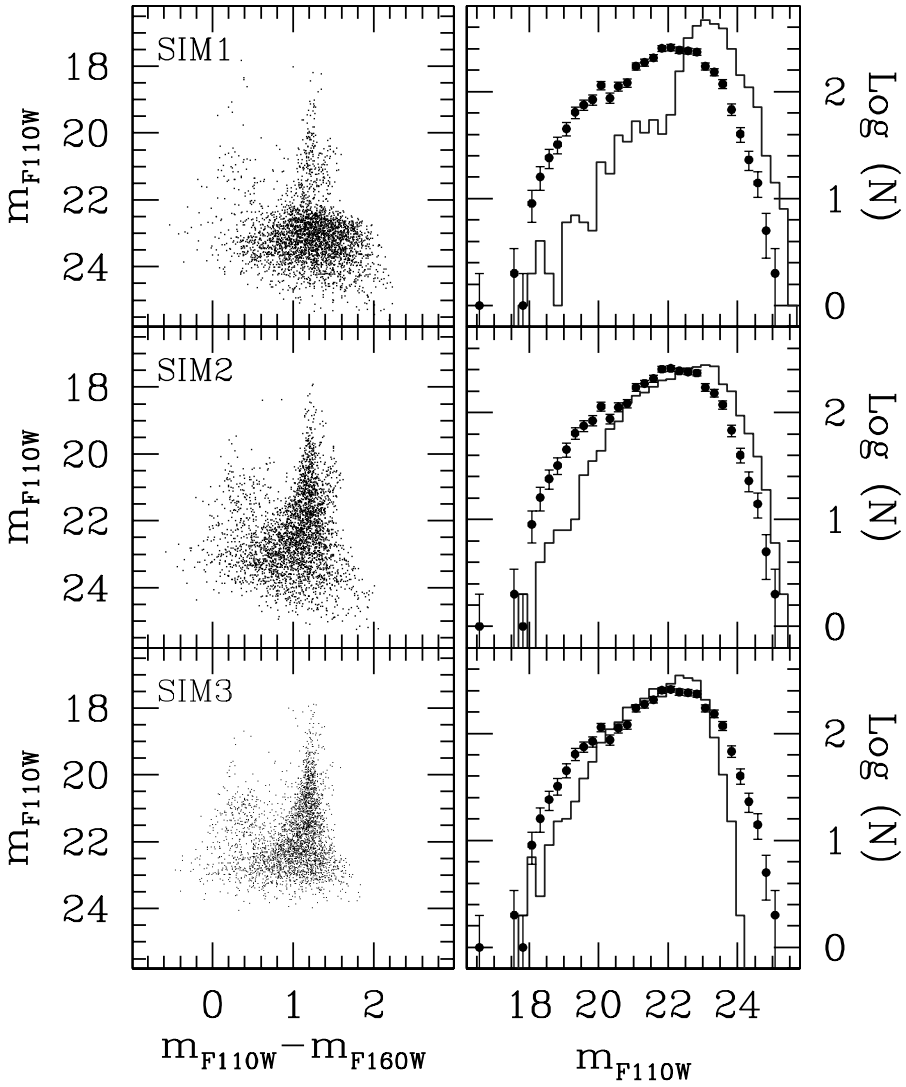

FIG. 3.—*Top*: SIM1, an old single episode. The galaxy forms stars from 5×10^9 yr ago until today. The mean SFR is 0.28 $M_\odot$ yr^{-1} kpc^{-2}. *Middle*: SIM2, a young single episode. In this case NGC 1569 forms stars from 5×10^8 to 1×10^7 yr ago with a mean SFR $\sim$ 1.1 $M_\odot$ yr^{-1} kpc^{-2}. *Bottom*: SIM3, a single episode that forms stars from 1.5×10^8 to 1×10^7 yr ago with an SFR of 1.7 $M_\odot$ yr^{-1} kpc^{-2}. [*See the electronic edition of the Journal for a color version of this figure*.]

stars in the observed CMD. Here we describe only three representative models: the first one (hereafter SIM1, plotted in Fig. 3) assumes a long SF activity, commencing 5 Gyr ago and still ongoing. The second model (hereafter SIM2, plotted in Fig. 3) assumes an SF commencing only 500 Myr ago and terminating 10 Myr ago. The third simulation (hereafter SIM3, plotted in Fig. 3) generates stars from 150 to 10 Myr ago.

SIM1 has an SFR of 0.28 $M_\odot$ yr^{-1} kpc^{-2} (0.01 $M_\odot$ yr^{-1}). The simulated objects are concentrated in the lower, fainter part of the CMD ($m_{F110W} \gtrsim 22.5$), where the low-mass stars in the RGB phase are located. The observed CMD does not show a similar concentration of objects in the faintest part. Conversely, at brighter magnitudes ($m_{F110W} < 22.5$) the synthetic red plume shows a star deficiency with respect to the observed LF. These inconsistencies show that the bulk of the assumed SF activity is located at excessively early epochs and provides too many old stars. At the same time the synthetic CMD is populated by blue massive stars (with $M > 20\ M_\odot$). A dozen of these synthetic stars are in the main-sequence phase. However, we cannot clearly distinguish the main sequence from the other evolved phases in the observed CMD because of the large photometric errors at faint magnitudes. We have also performed several simulations to overcome the small number statistics of the stars located at bright luminosity ($m_{F110W} < 18.5$). These simulations suggest that too many red supergiant stars are produced without observational counterparts. We can conclude that, in addition to the excess of old stars in the synthetic CMD, we also have an excess of young stars. This is the reason why in SIM2 we have turned on the SF more recently and turned it off earlier (10 Myr ago).

SIM2 has an SFR $\sim$ 1.1 $M_\odot$ yr^{-1} kpc^{-2} ($\sim$0.04 $M_\odot$ yr^{-1}) and fails to account for the brighter stars of the red plume. Again, at faint magnitudes SIM2 shows an excess of stars. In both simulations (SIM1 and SIM2), we have a feature in the region $19.5 < m_{F110W} < 21.5$ and $1.45 < m_{F110W} - m_{F160W} < 1.7$, which corresponds to stars with masses 4–6 $M_\odot$ in the AGB phase and does not appear in the observed CMD. We then tried to simulate the CMD with a single episode starting 1.5×10^8 yr ago and terminating 10 Myr ago in order to avoid these stars. SIM3 has an SFR of 1.7 $M_\odot$ yr^{-1} kpc^{-2} (0.07 $M_\odot$ yr^{-1}). This simulation avoids the feature obtained in SIM1 and SIM2 but shows a shortage of stars at low luminosities ($m_{F110W} > 23$) and at the top of the red plume ($m_{F110W} < 20$) and an excess of objects in the middle ($20 < m_{F110W} < 23$) of the luminosity function.

At the end of these preliminary simulations, no solution has been found that simultaneously fits both the bright and the faint parts of the CMD. Hence, a single episode cannot reproduce the observed CMD: to improve the fit to the data, we need to perform multiple-episode cases.

4.2. *Multiple-Episode SF*

We use the age-box procedure to investigate multiple episodes. The basic idea is that we can perform our analysis by dividing the CMD into regions (boxes) populated by stars with selected properties, such as age or evolutionary phase (Greggio 2002). A similar procedure is adopted by Gallart et al. (1996). The star counts in each box are directly linked to the mass that went into stars in the SF episodes that occurred at the corresponding epochs, i.e., the average SFR over the specific time intervals (Greggio 2002).

In order to better understand the age-box procedure, we introduce Figure 4, where we plot the apparent magnitude versus the age of red ($m_{\rm F110W} - m_{\rm F160W} > 0.9$) post–main-sequence stars. Vertical shading indicates He-burning stars and slanted shading indicates RGB (angle $= +45^\circ$) and E-AGB (angle $= -45^\circ$) stars. Because of the evolutionary lifetimes, the red stars at magnitudes brighter than 22.4 (where the tip of the RGB is located) are mostly core He–burning objects. The straight relation between their magnitude and age (Fig. 4, *thick shaded strip*) translates into a good temporal resolution of the SFH at ages younger than about 0.1 Gyr. This allows us to obtain precise results in the boxes corresponding to the top of the red plume. At magnitudes fainter than 22.4, each LF bin collects (in principle) stars with ages up to the Hubble time. The stellar counts in this region allow us to derive only integrated information.

In practice, we first define the magnitude ranges of the box by identifying the features in the LF[5] that suggest a possible discontinuity in the star formation. The color ranges are chosen in such a way as to account for the spread because of the photometric errors. These ranges constrain the box that defines our partial model, which is constrained to reproduce the observed stellar counts in the box with an SF activity within a specific age range. The limits for the age range are read from Figure 4 in correspondence to the magnitude limits of the box. Besides the objects in the box, the simulation also populates the diagram in regions different from the box described above; we take these "additional" objects into account when we perform the simulations in the other parts of the CMD. We have run hundreds of cases to infer the best combination of parameters. However, for the sake of clarity, here we simply describe the line of reasoning and show the most relevant results from all these tests. This method has been applied and extensively discussed by Schulte-Ladbeck et al. (2000, 2002), Crone et al. (2002), and Annibali et al. (2003).

4.2.1. *One-Box Simulations*

Following the above reasoning, we define the box (hereafter BOX1) in the magnitude range $18.5 < m_{\rm F110W} < 20.5$ (at $m_{\rm F110W} = 20.5$ a dip in the LF is noticeable) and colors $1.0 < m_{\rm F110W} - m_{\rm F160W} < 1.4$ (to take into account the photometric errors). Figure 4 shows that in BOX1 we are sampling core He–burning stars in the age range $(1–4)\times10^7$ yr; these objects are the youngest, most massive stars of the red plume. This box also includes a population of lower mass stars in the AGB phase; because of their short lifetimes in this magnitude range, these stars provide a minor contribution to the overall population.

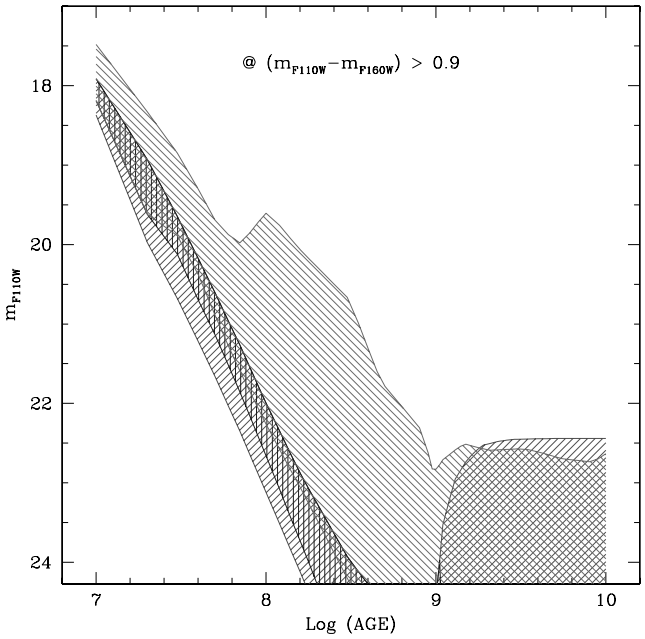

FIG. 4.—Magnitude range covered by red post–main-sequence stars of a simple stellar population with an age between 10 Myr and 10 Gyr selected in color $m_{\rm F110W} - m_{\rm F160W} > 0.9$. Vertical shading indicates He-burning stars and slanted shading indicates RGB (angle $= +45^\circ$) and E-AGB (angle $= -45^\circ$) stars. This plot clearly shows that the temporal resolution is worse at older ages. [*See the electronic edition of the Journal for a color version of this figure.*]

After many simulations, we find the best parameter combination (SIM4) that reproduces the number counts in BOX1 (Fig. 5). SIM4 is an episode commencing 3.7×10^7 yr ago and finishing 1.3×10^7 yr ago with a mean SFR of 3.1–3.3 $M_\odot$ yr^{-1} kpc^{-2} (0.12–0.14 $M_\odot$ yr^{-1}). We performed other simulations by slightly changing the boundary ages of the episodes for an estimate of the uncertainty affecting the determination of the age intervals.

Other possible solutions have a starting epoch in the range $(3.5-3.8)\times10^7$ yr ago and an ending epoch in the range $(1.3–1.4)\times10^7$ yr ago. In all the explored cases, the simulations for this young episode share a problem that is also visible in SIM4: an overproduction of stars with $m_{\rm F110W} - m_{\rm F160W} < 0.5$ (hereafter "blue bulk"). This structure corresponds to the blue edge of the blue loop phase of 8–12 $M_\odot$. We cannot remove this feature without underproducing the objects in the red plume. The number of objects generated in this recent SF episode is 20% of the total.

We then tried to simulate the remaining objects with a single episode, but we did not succeed in reproducing the LF. If we construct single episodes starting at epochs earlier than 3×10^8 yr ago and terminating 4×10^7 yr ago, we obtain too many faint objects ($m_{\rm F110W} > 22.5$) and too few stars in the range $m_{\rm F110W}$ 20.5–22.5 in the synthetic diagram. On the other hand, an episode that begins to form stars $\lesssim3\times10^8$ yr ago does not produce a sufficient number of objects at faint magnitudes.

The lack of success in reproducing the LF with only two episodes led us to consider other scenarios.

4.2.2. *Two-Box Simulations*

The second box (hereafter BOX2) is defined in the magnitude range $20.5 < m_{\rm F110W} < 22.5$ and color $0.9 < m_{\rm F110W} - m_{\rm F160W} < 1.3$ and targets the intermediate ages. The bright limit

[5] The comparison between model and data is performed selecting the red LF. However, in this paper we only report on the total luminosity function, since our CMD is mostly composed of a red population and the red LF does not significantly differ from the total one.

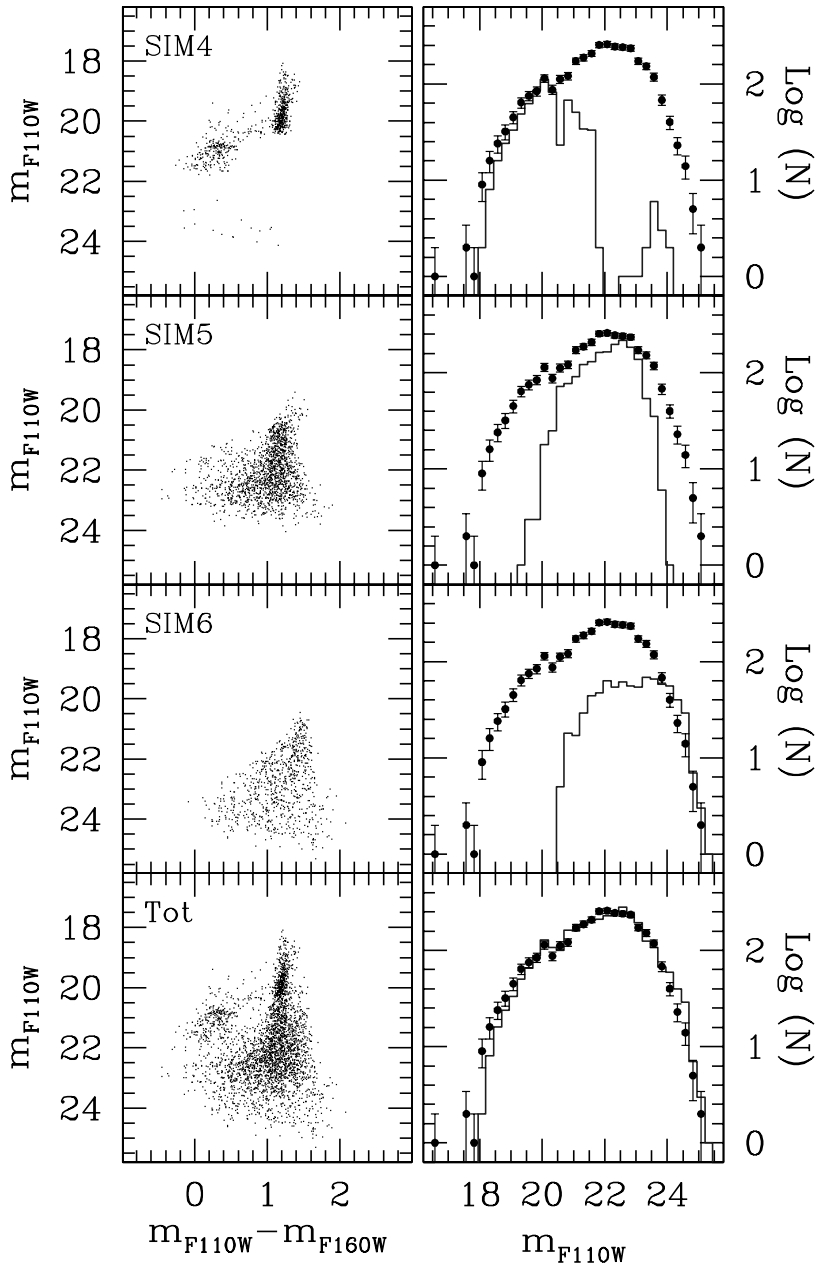

FIG. 5.—Best synthetic CMDs and luminosity functions. In the top panel the youngest episode (SIM4) that reproduces the objects in BOX1 is plotted. The galaxy experienced strong SF beginning 3.7×10^7 yr ago and terminating 1.3×10^7 yr ago with a high rate of $\sim3.2\,M_\odot$ yr^{-1} kpc^{-2}. In the second panel from the top we plotted the intermediate episode (SIM5) constrained by BOX2. This episode occurred in the interval $1.5\times10^8-4\times10^7$ yr ago with an SFR $\sim1.2\,M_\odot$ yr^{-1} kpc^{-2}. The oldest episode that reproduces the remnant objects (SIM6) is reported in the third panel from the top. The age interval is $6\times10^8-3\times10^8$ yr ago, and the SFR $= 1.5\,M_\odot$ yr^{-1} kpc^{-2}. The final composed synthetic CMD is drawn in the bottom panel. [*See the electronic edition of the Journal for a color version of this figure.*]

is fixed by BOX1, while the faint limit is chosen to be slightly brighter than the RGB tip in order to exclude possible blended RGB stars from the counts. From Figure 4, one can see that stars falling in BOX2 have ages in the range 1.2×10^8–4×10^7 yr if they are core He burners. The color limits of BOX2 were indeed chosen with the aim of isolating core He–burning stars, while taking into account the color spread due to photometric errors.

The best simulation for BOX2 (hereafter SIM5) accounts for ~50% of the objects and is plotted in the panels second from the top in Figure 5. SIM5 has a SFR $= 1.2\,M_\odot$ yr^{-1} kpc^{-2} ($0.04\,M_\odot$ yr^{-1}). This episode started forming stars 1.5×10^8 yr ago and terminated 4.0×10^7 yr ago. The starting epoch is older than the 1.2×10^8 yr mentioned above. When computing the simulations, we vary the starting and ending epoch around the values derived from Figure 4 in order to fit the observed LF with the minimum number of individual SF episodes. It turns out that starting at 1.5×10^8 yr allows us to fit the stellar counts in the range 22.5–23.5 without adopting a new box. Notice that at such magnitudes the completeness factors fall below 50%.

If we assume that a quiescent phase (or one with low SFR) occurred $(3.7-4)\times10^7$ yr ago, we can also reproduce the shape of the LF in the magnitude range m_{F110W} 20–20.5. This kind of short interburst phases has also been found by G98.

4.2.3. *The Remaining Objects*

The simulations computed to reproduce the stellar counts in BOX1 and BOX2 account for about 70% of the total number

of observed objects. The remaining 30% must be ascribed to SF that occurred at epochs older than 1.5×10^8 yr. From Figure 4, we see that the CMD in the magnitude range 22.5–24.5 can be populated with a mixture of relatively young He-burning stars [with ages of $(1.5-3)\times10^8$ yr], early-AGB (E-AGB) stars with intermediate ages (up to 1×10^9 yr), and RGB stars with ages up to the Hubble time. Therefore, we tested various starting epochs for the oldest episode of SF sampled by our data.

First, we attempted to account for the remaining stars by considering He-burning objects with ages between 3×10^8 and 1.5×10^8 yr. The simulation fits the LF fainter than $m_{\rm F110W} < 22.5$ reasonably well but yields too many stars in the region $19.5 < m_{\rm F110W} < 21$ at colors $1.45 < m_{\rm F110W} - m_{\rm F160W} < 1.7$. The overproduction amounts to a factor of 4–5. These are bright E-AGB stars with masses between 4 and 6 $M_\odot$. As discussed in § 4.1, these synthetic objects were also produced in SIM2, which assumed active SF at intermediate ages. If we use the number counts in the box $19.5 < m_{\rm F110W} < 21$; $1.45 < m_{\rm F110W} - m_{\rm F160W} < 1.7$ to constrain the SF activity at ages between 1.5×10^8 and 3×10^8 yr ago, we obtain an SFR level of 0.14 $M_\odot$ yr^{-1} kpc^{-2} (0.006 $M_\odot$ yr^{-1}), which is 1 order of magnitude lower than the rate of NGC 1569 in the young and intermediate episodes. We then tested SF episodes setting in at various epochs, but all ending 3×10^8 yr ago, to avoid the overproduction of these bright AGB stars. We found that if the old SF episode started a few Gyr ago, the upper RGB stands out very clearly on the synthetic CMD, with a prominent horizontal feature corresponding to the tip. This is not seen in the data. For a starting epoch of 2×10^9 yr ago, the signature of the RGB tip is no longer apparent, and we obtain consistency with both the CMD and the LF.

We obtain acceptable models for any starting epoch in the range 2–0.6 Gyr, with corresponding variations of the SFR. For example, a simulation started 1.5×10^9 yr ago yields an SFR of 0.4 $M_\odot$ yr^{-1} kpc^{-2} (0.009 $M_\odot$ yr^{-1}); a simulation started 6×10^8 yr ago yields SFR = 1.5 $M_\odot$ yr^{-1} kpc^{-2} (0.06 $M_\odot$ yr^{-1}). Our best fit is actually the latter, since the former case tends to underproduce the faint AGB stars, corresponding to 3 $M_\odot$ objects ($20.5 > m_{\rm F110W} > 21.5$) . The best simulation for the remaining objects is shown in Figure 5 as SIM6, while the best composite CMD is plotted in Figure 5 with the label Tot.

4.3. *Searching for Other Parameter Combinations*

We have performed many other simulations in order to search for alternative solutions; in particular, we considered cases with different IMFs, with slope α in the interval 1.35–3.35. Figure 6 plots the SFR as a function of the IMF exponent for the youngest (*circles*) and intermediate (*triangles*) episodes. Figure 6 also shows that the SFR has a minimum at $\alpha_{\rm min} \simeq 1.5-2$. This behavior is due to the nonlinear relation between the slope of the IMF and the number of stars per unit mass of the parent stellar population. By adopting a steep IMF (e.g., $\alpha \simeq 3$), the low-mass stars are relevant in number and weight with respect to the total population, while the contribution of high-mass stars to the total mass is negligible. For a flat IMF (e.g., $\alpha \simeq 1.3$), low-mass stars are still numerous, but their weight decreases. On the other hand, the number of massive objects become slightly higher, but their contribution to the total mass increases more than the total number.

We can broadly reproduce the shape of the LF in BOX1 with an IMF flatter than Salpeter's (down to $\alpha = 1.35$). For simplicity, in this paper we have adopted a single-slope IMF, extending Salpeter's IMF to the mass range 0.1–120 $M_\odot$. Gould et al. (1997) suggest a slope flatter than Salpeter's ($\alpha = -0.56$) for $M < 0.6\ M_\odot$. Chabrier (2003) has also found that the IMF in the Galaxy depends weakly on the environment and is well described by a power law for $M \gtrsim 1\ M_\odot$ and a lognormal form below this mass, except possibly for early SF conditions. For the Galactic disk, Kroupa & Weidner (2003) found an IMF with a slope $\alpha = 1.3$ in the range 0.08–0.5 $M_\odot$ and a slope that is consistent with Salpeter's above 0.5 $M_\odot$. If we extrapolate the SFR at $M < 0.5\ M_\odot$ by adopting Kroupa's rather than Salpeter's IMF, the values become 30% smaller than with the default Salpeter IMF.

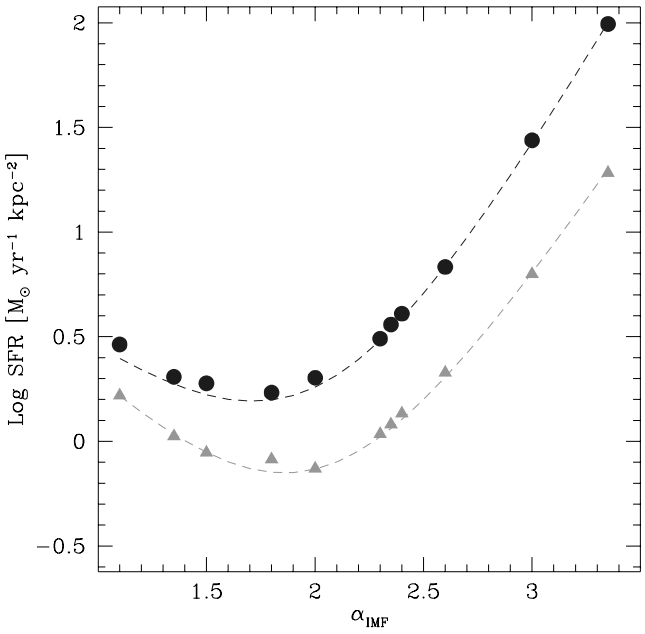

FIG. 6.—Trend of the SFR as a function of the IMF slope (α). Filled circles indicate the youngest episode (BOX1, $8\ M_\odot < M < 15\ M_\odot$), and filled triangles indicate the intermediate one (BOX2, $5\ M_\odot < M < 8\ M_\odot$). Dashed lines show the theoretical relation between the IMF slope and the SFR of the corresponding box. The differences are due to stochastic fluctuations. [*See the electronic edition of the Journal for a color version of this figure.*]

We have performed quantitative comparison (χ^2) between our best model and alternative solutions without the gap in the age range 37–40 Myr and found that the model with the gap is ~2000 times more probable than the fit without the gap.

Another possible SFH reproducing the brightest portion of the red plume consists of many short episodes in the age interval $(1-4)\times10^7$ yr ago. This possibility is also indicated by the "granularity" of the LF. In this case we obtain the best fit with three episodes separated by short periods (few million years) of quiescence or very low SFR. SIM4a started 2.1×10^7 yr ago and terminated 1.3×10^7 yr ago with an SFR of ~4.2 $M_\odot$ yr^{-1} kpc^{-2} (~0.18 $M_\odot$ yr^{-1}); SIM4b started 3.0×10^7 yr ago and terminated 2.2×10^7 yr ago with an SFR of ~4.5 $M_\odot$ yr^{-1} kpc^{-2} (~0.19 $M_\odot$ yr^{-1}); SIM4c started 3.7×10^7 yr ago and terminated 3.3×10^7 yr ago with an SFR of ~3.2 $M_\odot$ yr^{-1} kpc^{-2} (~0.13 $M_\odot$ yr^{-1}). This SFH reproduces remarkably well the brightest portion of the total LF. These three episodes have SFRs equal or higher than the single episode (see SIM4), but their total astrated mass is similar to that. We prefer not to pursue this fine tuning (although we cannot exclude a more complex scenario in the recent star formation) because the shape of the red plume and its LF may be affected by residual starlike systems mistaken as individual stars in spite of all our checks (see AL01) .

There are no clear evolutionary features in the observed CMD (Fig. 1) that allow a precise estimate of the distance modulus of

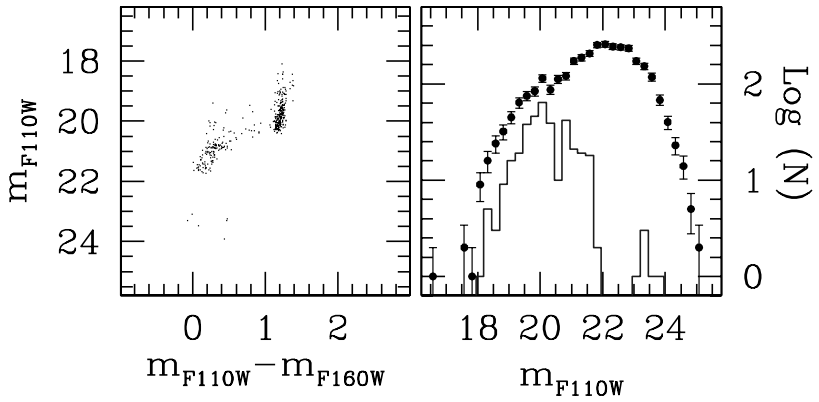

FIG. 7.—Simulation attempting to reproduce the number of objects in the box of the blue bulk. The number of objects at the top of the red plume is underestimated: this is an indication that the SFR found in SIM4 is an upper limit. [*See the electronic edition of the Journal for a color version of this figure.*]

the galaxy. Therefore, we have performed several simulations in order to examine the effects of changing the distance on the derived SFH in NGC 1569. To this end, we have adopted the lowest and the highest values of the DM found in the literature (DM = 26.1–27.3). In general, we obtain a different fit to the data by changing the DM. For sake of clarity, we only discuss the case of the larger distance, since this could be important in order to understand whether the RGB tip can be hidden. In this case, we derive a younger episode with higher SFR with respect to our best model. This is because a given apparent magnitude samples intrinsically brighter, and hence more massive, stars when DM is larger. As a consequence, a larger number of massive and young stars needs to be reproduced by the simulations. In addition, when we modify the distance of the galaxy we also change the position of the evolutionary features of the synthetic CMD. This effect is important because it could substantially modify the SFH. By adopting DM = 27.3, the best fit is obtained with a young episode that has formed objects in the age interval 2.7×10^7–8×10^6 yr ago, and the intermediate SF occurred 1×10^8–3.2×10^7 yr ago. The corresponding SFRs are about 2 times higher than those found for DM = 26.71 in SIM4 and SIM5. An SF with a rate of 0.8 $M_\odot$ yr^{-1} kpc^{-2} (0.04 $M_\odot$ yr^{-1}) that occurred in the age interval 1.3×10^9–2×10^8 yr ago is consistent with the data. We can exclude a strong SF occurring at ages older than 1–2 Gyr because the RGB tip would be clearly present in the CMD despite the higher distance. We want to stress again that, for what concerns the older SF, the results must be qualified by considering the uncertainties at faint magnitudes because of the incompleteness and photometric errors.

The reddening uncertainty suggested by the spread of the literature values shifts the synthetic CMD by 0.05 in color ($m_{F110W} - m_{F160W}$) and 0.1 in magnitude (m_{F110W}); its effect on the age of the episodes is smaller than those due to the uncertainties on the distance modulus and tracks.

Finally, with the synthetic CMD method, we can provide hints on the metallicity of the SF episode. Our capability to select the metallicity of an episode depends on the photometric errors relative to its main evolutionary phase. In principle, we are able to reject all the metallicities that create unobserved features in the synthetic CMD. The colors of the red plume are best reproduced with $Z = 0.004$; the $Z = 0.0004$ tracks yield red supergiants that are too blue compared to the observations. The $Z = 0.008$ tracks instead produce very red objects. At fainter magnitudes, where the photometric errors are larger, the presence of a low-Z population cannot be ruled out, while the $Z = 0.008$ tracks produce stars that are too red with respect to the data.

4.4. *Observational and Theoretical Uncertainties*

The low Galactic latitude of NGC 1569 ($b \sim 11\overset{\circ}{.}2$) led us to check the number of Milky Way stars falling into our field of view. AL01 ran the Galaxy model described by Casertano et al. (1990) and found that the foreground contamination in our (small) analyzed region is negligible. Major problems in our analysis are instead crowding, the shallow limiting magnitude, and the high reddening. Crowding is severe in the central region because the high recent SF activity has generated many bright, young objects that hide fainter, older ones. In addition, the shallow limiting magnitude does not allow us to reliably detect features that could help us to better determine the characteristics of the older episode. From this point of view, despite the high reddening, deeper, higher resolution *HST* images in optical bands could have possibly provided a better data set to study the earlier epochs. This has been clearly demonstrated by Annibali et al. (2003) in NGC 1705 (a BCD twice as distant as NGC 1569). In that case, WFPC2 photometry has allowed us to reach 1–1.5 mag below the RGB tip in regions where NIC2 barely allows the identification of the tip.

An additional uncertainty on the analysis of the central region of NGC 1569 comes from the presence of many small clusters (Hunter et al. 2000; Anders et al. 2004) and starlike systems. Most of them appear as bona fide stellar objects in our photometry, with shape, sharpness, and χ^2 parameters typical of single stars. These unresolved systems could be located in the CMD at the top of the red plume. By keeping or removing all possible cluster candidates from our empirical CMD, we estimate that the starlike systems could change the SFR by 15%–20% and shift the end epoch of the youngest episode to an age a few Myr older.

As discussed above and shown in the top panels of Figure 5, what we called blue bulk in § 4.2 could affect the derivation of the SFR of the youngest episode. This spurious feature could be due either to uncertainties in the bolometric corrections in the infrared filters or to uncertainties in the stellar tracks at the blue edge of the blue loops for the masses 8–12 $M_\odot$. In order to evaluate the influence of the blue bulk, we resimulated the top of the red plume by locating a box in the region of the blue bulk ($20.5 < m_{F110W} < 21.5$ and $0.9 < m_{F110W} - m_{F160W} < 1.3$). By using the same age interval as that of the youngest episode, the simulation generates a partial model, plotted in Figure 7, which provides an SFR of 1.6 $M_\odot$ yr^{-1} kpc^{-2} (0.06 $M_\odot$ yr^{-1}). This simulation is able to generate only 50% of the total objects in the red plume of the observed CMD and is clearly inconsistent

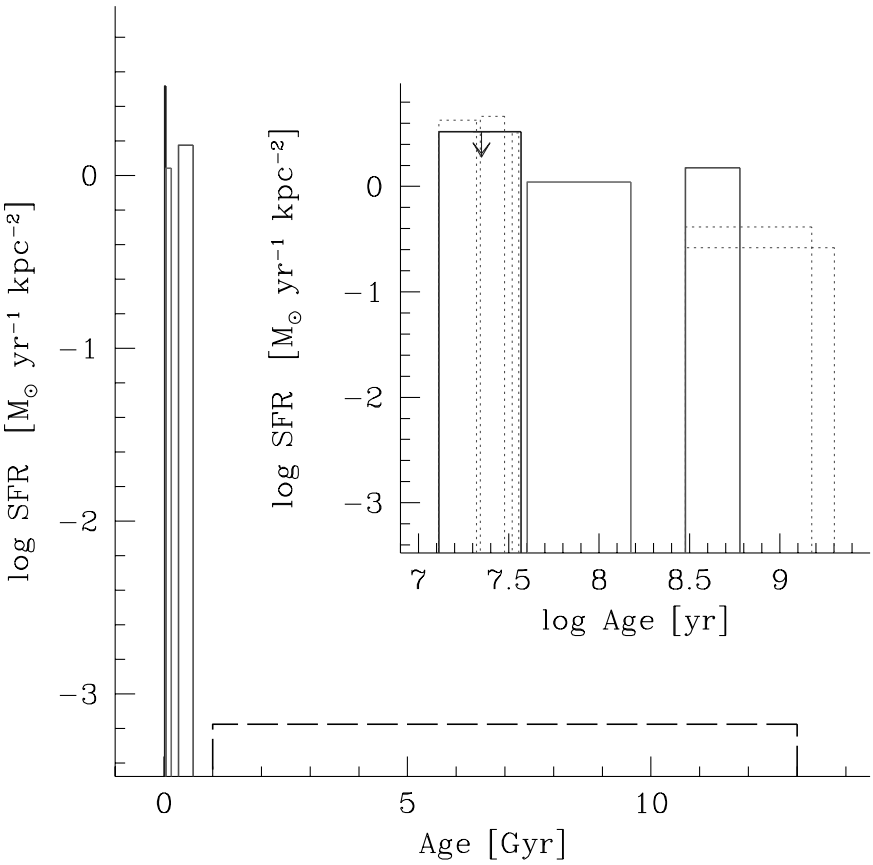

FIG. 8.—Derived SFH of NGC 1569. The SFR over the Hubble time is reported in the main plot linearly in age. The solid lines refer to the episodes of Fig. 5, and the dashed line refers to the second scenario described in the conclusions. The recent star formation history resulting from the simulations is shown in the small logarithmic plot. We give only an upper limit for the youngest episode. These uncertainties in the SFR are due to the blue bulk feature. Dotted lines indicate other possible solutions described in the text. [*See the electronic edition of the Journal for a color version of this figure.*]

with the data. We also performed many simulations by using Padova tracks of different metallicity, but we found similar problems. In other words, either we reproduce the number of stars in the blue bulk region but severely underproduce the red plume objects, or we reproduce the red plume and overestimate the blue bulk. We consider the latter option more viable, since the timescales of stellar evolution models at the blue edge of the blue loops are more uncertain than those of the red plume phases. Notice that Greggio et al. (1998) have derived the SFH in the B and V bands, adopting both the Geneva and Padova tracks in order to evaluate the uncertainty related to different stellar evolutionary models. They found an excess of synthetic stars at the blue edge of the blue loop with the Geneva tracks but not with the Padova tracks. This suggests that an additional uncertainty comes into play in the blue bulk; for instance, the completeness factor could be overestimated because its color dependence has not been considered in the simulations.

5. DISCUSSION AND CONCLUSIONS

The best agreement between the simulations and the data is obtained by adopting the SFH plotted in Figure 8 (*solid line*). Keeping in mind that these results are affected by many uncertainties (both in data and models), we can derive the following overall scheme for the SFH of NGC 1569. (Recall that the results described in this paper refer to the central region of the galaxy.)

1. NGC 1569 has experienced a complex SFH, composed of at least three strong episodes in the last 1 (possibly 2) Gyr.

2. The quiescent phase that occurred $(1.5-3)\times10^8$ yr ago is inferred from the small number of 3–6 $M_\odot$ stars in the AGB phase.

3. We need an episode older than 3×10^8 yr to reproduce the fainter part of the CMD. This old SF may have started as early as 1–2 Gyr ago. The large uncertainties (severe incompleteness, large photometric errors) that characterize the fainter part of the CMD do not allow us to infer reliable details on the SF of the oldest episode. However, we find hints for a significantly lower SF activity (or even a quiescent phase) at ages older than 1–2 Gyr (for a distance of 2.2 Mpc).

4. A Salpeter IMF reproduces the brighter parts of the observed CMD and the LF reasonably well. A flatter IMF is also able to reproduce the brighter portion of the red plume.

5. By assuming a Salpeter IMF over the whole mass range, the most recent SF occurs at a rate of 3.1–3.3 $M_\odot$ yr^{-1} kpc^{-2} (0.12–0.14 $M_\odot$ yr^{-1}), the intermediate one at a rate of 1–1.2 $M_\odot$ yr^{-1} kpc^{-2} (0.03–0.05 $M_\odot$ yr^{-1}), and the older one at a rate between 0.25 and 1.5 $M_\odot$ yr^{-1} kpc^{-2} (0.01–0.06 $M_\odot$ yr^{-1}), depending on the assumed duration.

6. The uncertainties of the distance modulus affect the estimates of the ages and SFRs of the episodes. The best fit obtained with a larger distance of DM = 27.3 is $2.7\times10^7-8\times10^6$ yr ago for the young and $1\times10^8-3.2\times10^7$ yr ago for the intermediate episode. The corresponding SFRs are about 2 times higher than those found for DM = 26.71. An SF with a rate of 0.8 $M_\odot$ yr^{-1} kpc^{-2} (0.04 $M_\odot$ yr^{-1}) occurred in the age interval $1.3\times10^9-2\times10^8$ yr ago. In addition, for the larger distance we can exclude

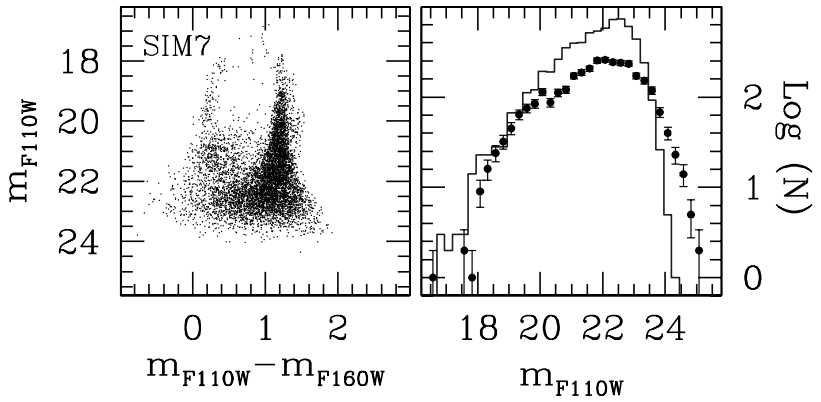

FIG. 9.—Simulation of an episode with duration and SFR as found by G98. These parameters do not allow us to reproduce the observed CMD and LF. [*See the electronic edition of the Journal for a color version of this figure.*]

a strong SF that occurred at ages older than 1–2 Gyr because the RGB tip would be clearly present in the CMD.

7. We cannot exclude more than one SF episodes occurring in the age interval $(1-4)\times10^7$ yr. A possible scenario could consist of three episodes with an SFR of 4.2, 4.5, and 3.2 $M_\odot$ yr^{-1} kpc^{-2} (0.18, 0.19, and 0.13 $M_\odot$ yr^{-1}) separated by short phases of quiescence or low activity. The uncertainties are due to the possible presence of clusters at the top of the red plume and small number statistics.

By comparing our results and those from the literature for the SFH of NGC 1569, we find overall agreement, although with interesting differences. The end of the youngest episode (1.3×10^7 yr ago) is significantly older than that obtained by Vallenari & Bomans (1996) and G98, who place it around $(5-10)\times10^6$ yr ago, as found from optical *HST* data. These differences can be explained in terms of a different sensitivity of the different bands (optical vs. NIR) to hot and cold evolutionary phases. Here we are studying young massive stars with NIR data. We are then sensitive to the post–main-sequence phases, where these stars have very short lifetimes. Optical data, more appropriate for main-sequence objects, allow for higher reliability on the youngest stars. On the other hand, the NIR analysis allows us to distinguish the two recent episodes, separated by a short quiescent period, better than with the optical data. In addition, we find evidence for a gap, or a low SF, from 3×10^8 to 1.5×10^8 yr ago, similar to that suggested by Vallenari & Bomans (1996).

The SFR derived by G98 using the PC camera (which covers an area of 374 pc$\times$374 pc for a distance of 2.2 Mpc), is 4 $M_\odot$ yr^{-1} kpc^{-2} in the age interval $1.5\times10^8-5\times10^6$ yr ago. From Figure 8, we can see that our rate for the youngest episode (SIM4) is slightly lower than that derived by G98. For the intermediate episode, we have derived an SFR 3–4 times lower than G98. We performed further simulations by adopting the ingredients suggested by the literature cited above in order to better understand these differences. We cannot reproduce the top of the red plume if we simulate the totality of objects in the CMD with a continuous and constant activity starting $(1-1.5)\times10^8$ yr ago and ending 5×10^6 yr ago. Furthermore, this simulation underestimates the fainter part of the LF. Another simulation (SIM7, plotted in Fig. 9) assumes the SFR of G98 in the same age interval. The resulting synthetic diagram has twice as many stars than our observed CMD. The total luminosity function is broadly fitted in the brighter part of the red plume but shows an overabundance of objects in the range $m_{F110W}=19.5-23.5$, whereas the fainter part is barely populated. From the comparison of the observed LF with that from SIM7, we can learn that

1. If we terminate the SF 5×10^6 yr ago, we produce many high-mass stars without observed counterparts;

2. In the BOX1 area, SIM7 produces a number of objects $\sim$1.5 times higher than SIM4. Nevertheless, the SFRs of SIM7 and SIM4 are quite similar within the uncertainties, since the lengths of the two simulations are slightly different.

3. The simulated objects of SIM7 in the BOX2 region are about 3–4 times higher than SIM5 (this value is similar to the ratio of the corresponding SFRs). This discrepancy could arise from the uncertainties in the photometric error distribution and completeness factors used in this work and in G98. In addition, the differences in the SFH could result from the differences in the areas sampled by the two cameras.

By using archival *HST* data, Anders et al. (2004) find a high level of star cluster formation for ages younger than 2.5×10^7 yr and a lower level of star cluster formation at older epochs, with a secondary peak about 100 Myr ago. The cluster age distribution shows a gap in the age interval $(1.6-4.0)\times10^8$ yr. These results match our SFH that refers to field stellar population. However, Anders et al. (2004) find a younger age for the end of the last episode, consistent with the results by Vallenari & Bomans (1996) and G98. This again suggests that the optical data are more appropriate for studying the most recent epochs.

In order to estimate whether the expanding superbubbles can be plausibly driven by the observed population of massive stars, Heckman et al. (1995) found that the observations can be reproduced reasonably well by assuming an episode with a constant SF over the ages $(1.3-3.2)\times10^7$ yr ago. The ages of the episode are rather similar to our youngest burst.

By using population synthesis models, Belczynski et al. (2004) have constructed synthetic X-ray binary populations for direct comparison with the X-ray LF and found two principal stellar populations. One is old, metal-poor, with continuous SF from 1.5 Gyr ago, and the other is recent and metal-rich. Their results are consistent with ours for the oldest episode but invoke a recent burst younger than that inferred here. Again, we attribute our earlier termination to the selection effect, which makes it difficult to detect blue young stars in the NIR. We remind the reader that the most recent termination epoch for the SF inferred in the optical by G98 only refers to the regions of NGC 1569 where single stars were resolved. There are zones in this galaxy occupied by giant H II region complexes where even with the *HST* WFPC2 we were unable to resolve individual stars. The existence of these H II regions clearly suggests that the SF activity must have continued until even more recent times.

All three episodes have SFRs higher by 2–3 orders of magnitude than that of the solar neighborhood (e.g., Timmes et al. 1995) and than those inferred with similar methods in other late-type dwarfs (both irregulars and BCDs; see the reviews by Schulte-Ladbeck et al. 2001 and by Tosi 2003). The only dwarf analyzed so far with the synthetic CMD method that has an SFR comparable to that of NGC 1569 is NGC 1705 (Annibali et al. 2003). These two dwarfs, in spite of being classified differently (NGC 1705 is a BCD), have quite similar properties, all somehow related to the strong SF activity. They both contain SSCs, show evidence of galactic winds, and have SFRs consistent with those required by Babul & Ferguson (1996) to let dwarfs account for the excess of blue galaxies at intermediate redshift. Neither shows evidence of long quiescent phases in the last couple of Gyrs.

At the rates derived in this paper, the central region of NGC 1569 has formed $\sim 2.7\times10^7\ M_\odot$ of stars in the last 1 Gyr, i.e., about 8% of the total mass estimated by Israel (1988) and about 14% of the mass that is not associated with neutral hydrogen ($M_{\rm dif} = 2\times10^8\ M_\odot$). The field of view of NIC2 corresponds to an area of 0.04 kpc^2, which covers only $\sim$2.5% of the optical size of NGC 1569 (1.76 kpc^2; Israel 1988).

To improve our knowledge of the SF history, we have compared the integrated optical and infrared fluxes of the whole field and of the resolved stars in the NICMOS area from the images described by G98 and AL01. The integrated magnitudes in the *HST* F439W, F555W, F110W, and F160W filters are 13.7, 12.9, 10.9, and 10, respectively, for the field;[6] they are 15.2, 14.5, 12.1, and 11 for the resolved stars. The dereddened $m_{\rm F439W} - m_{\rm F160W}$ color of our investigated region is then $\simeq$1.6, noticeably bluer than the corresponding color for a solar Kurucz model [Kurucz 1992; $(m_{\rm F439W} - m_{\rm F160W})_\odot \simeq 2.2$]. The apparent integrated B magnitude of our NICMOS field is $m_{B,\rm NICMOS} \simeq 13.6$, while the total B magnitude of NGC 1569 is $m_B = 11.86$ (de Vaucouleurs et al. 1991). Hence, our NICMOS frame samples $\sim$20% of the total B light from the galaxy if the average reddening of the NICMOS region is representative of that of the whole galaxy. Note that our sampled area is only 2.5% of the total; therefore, the SF per unit area in NGC 1569 is very centrally concentrated.

We can explore some possible scenarios in order to place constraints on the past history of NGC 1569. Given the total and H I masses of NGC 1569 estimated by Israel (1988) and the astrated mass in the last 1 Gyr extracted from our CMD procedure and assuming a Salpeter's IMF over the whole mass range, we are left with only $1.73\times10^8\ M_\odot$ for the whole galaxy for the sum of the older stars and the dark matter. Assuming that these old stars were produced at a constant rate over the interval 1.3×10^{10}–1×10^9 yr ago, the corresponding SFR is $1.44\times10^{-2}\ M_\odot\ {\rm yr}^{-1}$. Since this SFR refers to the whole galaxy, the normalized value is $8.2\times10^{-3}\ M_\odot\ {\rm yr}^{-1}\ {\rm kpc}^{-2}$. This value is comparable to what has been derived via simulations for dwarf galaxies in the Local Group (see G98 and references therein). For the NIC area, the corresponding astrated mass over the age interval is $M_{\rm NIC} = 4.3\times10^6\ M_\odot$. If we simulate an episode that generates the $M_{\rm NIC}$ mass over the age interval reported above, we obtain a synthetic CMD that contains 5%–10% of the total objects of the observed CMD. These synthetic stars are on the RGB. Hence, in this scenario we cannot rule out that a constant but low SF might have occurred over the Hubble time.

However, it would be very unusual for a galaxy of this type to have a dark/visible mass ratio much lower than 10. Moreover, chemical evolution models (Romano et al. 2005) show that without the usual dark matter ratio, NGC 1569 would experience too early strong galactic winds and it would be impossible to reconcile the model predictions with the observational data.

In the second scenario (Fig. 8, *dashed line*) we therefore assume that the stellar component is only 10% of the dynamical mass; thus, our astrated masses are probably inconsistent with a Salpeter's IMF extrapolated down to 0.1 $M_\odot$. However, if we adopt a Kroupa & Weidner (2003) IMF, the central region has generated only $\sim$60% of the stellar mass of the galaxy over the last 1 Gyr. The resulting mean SFR over the interval 1.3×10^{10}–1×10^9 yr ago is $6.7\times10^{-4}\ M_\odot\ {\rm yr}^{-1}\ {\rm kpc}^{-2}$. Alternatively, considering an onset of the SF 7 Gyr ago (i.e., the galaxy started to form stars at redshift 1 by adopting the "concordance cosmology": $H_0 = 70$, $\Omega_\lambda = 0.7$, and $\Omega_M = 0.3$), the mean SFR is about 2 times higher than the value above. All these quantities lie in the range of SFRs typical for nearby dwarf galaxies. These scenarios do not allow us to rule out a past SF with a low rate (or similar to the typical SFR of the other dwarf galaxies), but we can safely conclude that the last 1–2 Gyr have been peculiar.

What could be the cause of this peculiar SF in the last Gyr? Interestingly, there is an H I cloud with mass $7\times10^6\ M_\odot$ located at a projected distance of 5 kpc from NGC 1569. It is connected to the galaxy by a bridge similar in mass to the H I cloud (Stil & Israel 1998). This cloud may have triggered the star formation (Stil & Israel 1998). Moreover, according to Muehle (2003), who studied the galaxy with high-resolution H I data, the structure of the galaxy halo is the remnant of an intergalactic H I cloud in the process of merging with the galaxy. If true, this may provide both the cause and the fuel for the strong and concentrated SF activity of NGC 1569.

To better understand the history of this intriguing object, we should try to resolve its stars older than the few Gyr reached by our current data, in both the inner and outer regions. Although the NIR bands are important to explore old stellar population, NICMOS is not an optimal instrument. The detection of the tip of the RGB (if it exists) will be achievable only with the *HST* Advanced Camera for Surveys, which has both the necessary spatial coverage and resolution.

We thank Francesca Annibali, Cristian Vignali, Paolo Montegriffo, Livia Origlia, Marcella Maio, and Lucia Pozzetti for their help and useful discussions. The authors also thank the anonymous referee for useful suggestions. This work has made use of the NASA Astrophysics Data System, the arXiv.org e-print archive, and the NASA/IPAC Extragalactic Database. This work has been partially supported by the Italian ASI, through grant 2002-IT059, and MIUR, through Cofin 2000.

[6] These values do not include the flux from the SSCs and from the H II regions, which were masked on the frames.

REFERENCES

Aloisi, A., et al. 2001, AJ, 121, 1425 (AL01)
Anders, P., de Grijs, R., Fritze-v. Alvensleben, U., & Bissantz, N. 2004, MNRAS, 347, 17
Annibali, A., Greggio, L., Tosi, M., Aloisi, A., & Leitherer C. 2003, AJ, 126, 2752
Arp, H., & Sandage, A. 1985, AJ, 90, 1163
Asplund, M., Grevesse, N., Sauval, A. J., Allende Prieto, C., & Kiselman, D. 2004, A&A, 417, 751
Babul, A., & Ferguson, H. C. 1996, ApJ, 458, 100
Belczynski, K., Kalogera, V., Zezas, A., & Fabbiano, G. 2004, ApJ, 601, L147
Burstein, D., & Heiles, C. 1984, ApJS, 54, 33
Casertano, S., Ratnatunga, K. U., & Bahcall, J. N. 1990, ApJ, 357, 435
Chabrier, G. 2003, PASP, 115, 763
Crone, M. M., Schulte-Ladbeck, R. E., Greggio, L., & Hopp, U. 2002, ApJ, 567, 258

De Marchi, G., Clampin, G., Greggio, L., Leitherer, C., Nota, A., & Tosi, M. 1997, ApJ, 479, L27
D'Ercole, A., & Brighenti, F. 1999, MNRAS, 309, 941
de Vaucouleurs, G., de Vaucouleurs, A., Corwin, H. G., Jr., Buta, R. J., Paturel, G., & Fouqué, P. 1991, Third Reference Catalogue of Bright Galaxies (Berlin: Springer)
Devost, D., Roy, J., & Drissen, L. 1997, ApJ, 482, 765
Dolphin, A. E., et al. 2003, AJ, 126, 187
Ellis, R. S. 1997, ARA&A, 35, 389
Fagotto, F., Bressan, A., Bertelli, G., & Chiosi, C. 1994, A&AS, 105, 29
Fruchter, A. S., & Hook, R. N. 2002, PASP, 114, 144
Gallart, C., Aparicio, A., & Bertelli, G. 2002, in ASP Conf. Ser. 274, Observed HR Diagrams and Stellar Evolution, ed. T. Lejeune & J. Fernandes (San Francisco: ASP), 483
Gallart, C., Aparicio, A., Bertelli, G., & Chiosi, C. 1996, AJ, 112, 2596
Galliano, F., Madden, S. G., Jones, A. P., Wilson, C. D., Bernard, J. P., & Le Peinter, F. 2003, A&A, 407, 159
Gonzalez-Delgado, R. M., Leitherer, C., Heckman, T. M., & Cervino, M. 1997, ApJ, 483, 705
Gould, A., Bahcall, J. N., & Flynn, C. 1997, ApJ, 482, 913
Grebel, E. K. 1997, Rev. Mod. Astron., 10, 29
Greggio, L. 2002, in ASP Conf. Ser. 274, Observed HR Diagrams and Stellar Evolution, ed. T. Lejeune & J. Fernandes (San Francisco: ASP), 444
Greggio, L., Tosi, M., Clampin, M., De Marchi, G., Leitherer, C., Nota, A., & Sirianni, M. 1998, ApJ, 504, 725 (G98)
Heckman, T. M., Dahlem, M., Lehnert, M. D., Fabbiano, G., Gilmore, D., & Waller, W. H. 1995, ApJ, 448, 98
Hunter D. A., O'Connell, R. W., Gallagher, J. S., & Smecker-Hane, T. A. 2000, AJ, 120, 2383
Israel, F. P. 1988, A&A, 194, 24
Izotov, Y. I., & Thuan, T. X. 2004, ApJ, 602, 200
Izotov, Y. I., Thuan, T. X., & Lipovetsky, V. A. 1997, ApJS, 108, 1
Karachentsev, I. D., Tikhonov, N. A., & Sazonova, L. N. 1994, Astron. Lett., 20, 84
Kobulnicky, H. A., & Skillman, E. D. 1997, ApJ, 489, 636
Kroupa, P., & Weidner, C. 2003, ApJ, 598, 1076
Kurucz, R. L. 1992, in IAU Symp. 149, The Stellar Populations of Galaxies, ed. B. Barbuy & A. Renzini (Dordrecht: Kluwer), 225
Lisenfeld, U., Israel, F. P., Stil, J. M., & Sievers, A. 2002, A&A, 382, 860
Makarova, L. N., & Karachentsev, I. D. 2003, Astrophys., 46, 144
Martin, C. L., Kobulnicky, H. A., & Heckman, T. M. 2002, ApJ, 574, 663
Mateo, M. 1998, ARA&A, 36, 435
Muehle, S. 2003, Ph.D. thesis, Rheinische Friedrich-Wilhelms Univ.
O'Connell, R. W., Gallagher, J. S., & Hunter, D. A. 1994, ApJ, 433, 65
Olive, K. A., & Skillman, E. D. 2004, ApJ, 617, 290
Origlia, L., & Leitherer, C. 2000, AJ, 119, 2018
Origlia, L., Leitherer, C., Aloisi, A., Greggio, L., & Tosi, M. 2001, AJ, 122, 815
Richer, M. G., & McCall, M. L. 1995, ApJ, 445, 642
Romano, D., Tosi, M., & Matteucci, F. 2005, MNRAS, submitted
Salpeter, E. E. 1955, ApJ, 121, 161
Schulte-Ladbeck, R. E., Hopp, U., Drozdovsky, I. O., Greggio, L., & Crone, M. M. 2002, AJ, 124, 896
Schulte-Ladbeck, R. E., Hopp, U., Greggio, L., & Crone, M. M. 2000, AJ, 120, 1713
Schulte-Ladbeck, R. E., Hopp, U., Greggio, L., Crone, M. M., & Drozdovsky, I. O. 2001, Ap&SS, 277, 309
Skillman, E. D., et al. 2003, ApJ, 596, 253
Smecker-Hane, T. A., Cole, A. A., Gallagher, J. S., III, Stetson, P. B. 2002, ApJ, 572, 1083
Stil, J. M., & Israel, F. P. 1998, A&A, 337, 64
———. 2002, A&A, 392, 473
Timmes, F. X., Woosley, S. E., & Weaver, T. A. 1995, ApJS, 98, 617
Tosi, M. 2003, Mem. Soc. Astron. Italiana, 75, 103
Tosi, M., Greggio, L., & Annibali, F. 2002, in ASP Conf. Ser. 274, Observed HR diagrams and Stellar Evolution, ed. T. Lejeune & J. Fernandes (San Francisco: ASP), 529
Tosi, M., Greggio, L., Marconi, G., & Focardi, P. 1991, AJ, 102, 951
Tosi, M., Sabbi, E., Bellazzini, M., Aloisi, A., Greggio, L., Leitherer, C., & Montegriffo, P. 2001, AJ, 122, 1271
Vallenari, A., & Bomans, D. J. 1996, A&A, 313, 713
Waller, W. H. 1991, ApJ, 370, 144